

## TECHNICAL NOTE

CrossMark  
click for updatesCite this: *Anal. Methods*, 2016, 8, 6815Received 10th June 2016  
Accepted 12th August 2016

DOI: 10.1039/c6ay01654e

[www.rsc.org/methods](http://www.rsc.org/methods)

## Evaluation of a high-resolution micro-sized magic angle spinning (HR $\mu$ MAS) probe for NMR-based metabolomic studies of nanoliter samples†

Nghia Tuan Duong,<sup>a</sup> Yuki Endo,<sup>b</sup> Takahiro Nemoto,<sup>b</sup> Hiroshi Kato,<sup>b</sup>  
Anne-Karine Bouzier-Sore,<sup>c</sup> Yusuke Nishiyama<sup>ab</sup> and Alan Wong<sup>\*d</sup>

This study evaluates the performances of a recently introduced 1 mm HR $\mu$ MAS NMR probe for metabolic profiling of nanoliter samples. It examines essential NMR criteria such as spectral data qualities and repeatability, and experimental practicality. The report also discusses the difficulties related to the sample preparation in HR $\mu$ MAS experiments and considers possible solutions and improvements.

### Introduction

Nuclear Magnetic Resonance (NMR) is an inherently insensitive spectroscopic technique. For this reason, High-Resolution Magic Angle spinning (HR-MAS) NMR analysis for metabolic detection relies often on large sample quantities, typically up to 10–20 mg.<sup>1</sup> This is problematic when limited samples are available; for instance in studies of a specific phenotype within isogenic cells and organisms or of tiny diseased tissues for early diagnosis. Therefore, a microscopic MAS technology capable of analysing sub-milligram specimens would open a new analytical perspective for exploring the uncharted area in HR-MAS NMR-based metabolomics.

Even though a few micro-MAS ( $\mu$ MAS) technologies, such as the use of a piggy-back design<sup>2</sup> and a spinning resonator known as Magic Angle Coil Spinning (MACS),<sup>3,4</sup> emerged in the past decade, these approaches – along with the other commercial  $\mu$ MAS probes<sup>5–7</sup> – are designed for rigid solid materials, and they do not offer sufficient spectral resolution (2 ppb) for <sup>1</sup>H NMR metabolic investigations of microgram ( $\mu$ g) specimens. Not until Wong and co-workers introduced a high-resolution MACS resonator denoted as HRMACS.<sup>8</sup> The HRMACS technique has found some preliminary success in metabolic profiling and differentiation of intact cells<sup>9</sup> and whole small organisms.<sup>10</sup> However, the HRMACS experiment is impractical. The HRMACS microcoil is a fragile component, and the fabrication and

manipulation of the coil require great efforts. Moreover, the effect of spinning on the microcoil often deteriorates the detection over time leading to erroneous interpretations. As a result, HRMACS is only applicable to simple 1D <sup>1</sup>H NMR profiling with a small sampling size. Finally, the presence of <sup>1</sup>H aliphatic background signals<sup>10</sup> prevents analyses of neighbouring metabolite signals such as lactate, valine and isoleucine.

Recently, a stand-alone 1 mm high-resolution  $\mu$ MAS probe (HR $\mu$ MAS) was introduced.<sup>11</sup> Unlike in HRMACS, there is no coil manipulation. It is essentially a robust probe that has the capability of recording spectra with high resolutions up to 2 ppb and with excellent detection sensitivity for  $\mu$ g biospecimens. However, there is no detailed assessment reported on the use of HR $\mu$ MAS. Here, we present the first <sup>1</sup>H NMR-based metabolic differentiation analysis using the HR $\mu$ MAS probe. The study examines several important criteria for NMR-based metabolomic studies – such as spectral data quality and repeatability, and operational practicality – using a simple metabolic differential NMR analysis on two different rat extracts, the liver and brain. Taking advantage of the good metabolic stability of bio-extracts, we could evaluate the optimal spectral performances (resolution and detection sensitivity) and the sample preparation without being concerned about the sample degradation. Four replicates were sampled for each group and subjected to spectral relative standard deviation analyses for assessing the spectral data repeatability.

### Experimental

#### Perchloric acid bio-extract preparation

Before dissection, the rat was perfused with a mixed solution containing 750 mM glucose and 534 mM [<sup>3-<sup>13</sup>C</sup>] lactate (Cambridge isotope, 99% enrichment). Intravenous perfusion was carried out using a syringe pump that maintains a flux to ensure that glycaemia levels remain constant. The infusion was

<sup>a</sup>RIKEN CLST-JEOL Collaboration Center, Tsurumi, Yokohama, Kanagawa 230-0045, Japan

<sup>b</sup>JEOL RESONANCE Inc., 3-1-2 Musashino, Akishima, Tokyo 196-8558, Japan

<sup>c</sup>Centre de Résonance Magnétique des Systèmes Biologiques, CNRS-Université de Bordeaux, UMR5536, Bordeaux, France

<sup>d</sup>NIMBE, CEA, CNRS, Université Paris-Saclay, CEA Saclay, 91191, Gif-sur-Yvette, France. E-mail: alan.wong@cea.fr

† Electronic supplementary information (ESI) available. See DOI: 10.1039/c6ay01654e

monitored to obtain a time-decreasing exponential from 15 ml h<sup>-1</sup> to 1.23 ml h<sup>-1</sup> during the first 25 minutes, after which the rate was kept constant.<sup>12</sup> At the end of the infusion, the rat was euthanized by using cerebral-focused microwaves (5 kW, 1 s, Sacron8000, Sairem) for an immediate stoppage of all enzymatic activities and to avoid post-mortem artefacts such as anaerobic lactate production. The brain and liver were then rapidly removed and immersed in liquid nitrogen.

The frozen organs were weighed (brain 1.2 g and liver 2.2 g) and pulverized under liquid nitrogen with a mortar and pestle. A volume of 5 ml of 0.9 M perchloric acid was then slowly added to the liquid nitrogen, and the frozen droplets were immediately pulverized. The frozen mixture (perchloric acid and the organs) was transferred to a Dounce homogenizer and homogenized at 4 °C after thawing. The suspension was then centrifuged at 10 000 g for 20 min. The supernatant was neutralized with KOH to pH = 7.2, followed by centrifugation separating the precipitates and potassium perchlorate salts. The extracted supernatant was then freeze-dried.

Four replicate samples were prepared for each lyophilized sample by dissolving four portions of the sample in D<sub>2</sub>O: ranging from 6.17 to 6.51 mg of the liver in 150 µl D<sub>2</sub>O; and 25.39 to 27.25 mg of the brain in 200 µl. The resultant mean concentrations were 41 µg µl<sup>-1</sup> for the liver and 131 µg µl<sup>-1</sup> for the brain. It is noteworthy that the actual sample concentration was lower, because the resultant extract solutions contained visible white potassium perchlorate precipitates. The solutions were then centrifuged and only the supernatants were used in the HRµMAS NMR analyses.

### NMR sample preparation

The samples were prepared under a stereomicroscope with a set of tools designed for packing µg samples (Fig. S1 in ESI†). An empty Kel-F rotor was mounted onto a rotor holder for handling. The bio-extracts were pipetted into the rotor using a micropipette equipped with a 20 µl GELoader® tip (Eppendorf, US). The rotor sealing was ensured by using two Kel-F inserts and one Kel-F cap: the first insert was placed and aligned at the tip of the rotor using the handling tools and then gently pushed with a blunt-ended fine needle until it was fully inserted. The same procedure was repeated at the other end of the rotor, with the second insert. The rotor was sealed by inserting the Kel-F cap with a dedicated cap-sealing tool. The entire sample-preparation procedure took 20–30 minutes.

### NMR spectroscopy

<sup>1</sup>H HRµMAS NMR experiments were carried out reproducing the standard protocol for HR-MAS experiments of biospecimens.<sup>1</sup> The NMR measurements were performed on a standard-bore 14.1 T magnet equipped with an ECZ600R spectrometer (JEOL RESONANCE Inc., Japan) operating at 599.669 MHz. The MAS frequency was set between 2000 and 2500 Hz with a stability of less than ±20 Hz. The experiments were performed under a <sup>2</sup>H-lock. The sample temperature was maintained constant at 13.0 ± 0.2 °C by using a variable-temperature unit. The B<sub>0</sub> field shimming was performed on a sucrose-D<sub>2</sub>O

solution prior to the study. The spectral data were recorded with a standard t<sub>2</sub>-filter Carr–Purcell–Meiboom–Gill (CPMG) experiment using a 90°-pulse of 1.3 µs (with 18 W) and a 20 µs echo-delay with a total CPMG echo time of 20 ms. A continuous-wave pulse was applied during the 2 s recycle delay for water suppression. A total of 32 768 data points were acquired using a spectral width of 25 ppm. The total data acquisition time for one-scan was 3.1 s. 128 scans were accumulated for each data point of the brain extract (7 minutes) and 512 scans for the liver extract (27 minutes). The <sup>1</sup>H chemical shifts were internally referenced to the internal lactate -CH<sub>3</sub>- doublet at δ = 1.33 ppm. Before the spectral data analyses, all spectra were processed with a 0.8 Hz line-broadening exponential apodization.

### Spectral variation analysis

To evaluate the spectral variation within the dataset, spectral relative standard deviation (RSD) analyses were carried out.<sup>13</sup> The RSD for each individual spectral bucket of the normalized spectral region 1.00–4.75 ppm was calculated. The bucketed (Δ = 0.01 ppm) NMR spectra were treated with a noise removal procedure, in which each bucket spectrum was divided into 32 subsections and the standard deviation (SD) of each section was calculated. The level of the noise for a given spectrum was estimated to be 3 times the smallest standard deviation. The spectral bucketing was performed using MestReNova, and the RSD calculations and processings were carried out using MATLAB.

### Multivariate data analysis

To reduce the complexity of the NMR data for multivariate analyses, the spectra were reduced to 0.005 ppm wide buckets over the spectral region between 0.5 and 9.0 ppm, with an exclusion of the water region 4.75–5.00 ppm. Before the multivariate data analysis, the bucketed spectra were normalized by the total sum of intensities. Principal component analysis (PCA) and orthogonal partial least-squares discriminant analyses (OPLS-DAs) were performed using SIMCA-P 13 (Umetrics, Umea, Sweden). All variable data were centred before PCA and OPLS-DAs.

## Results and discussion

### Probe practicality and performance

Similar to a 4 mm HR-MAS probe, the HRµMAS is a robust and convenient probe with most of the standard probe specifications. It is designed to reproduce the current HR-MAS experimental protocol for NMR-based metabolomic analyses.<sup>1</sup> The NMR experiment applied in this study was performed under a controlled environment: with a probe temperature of 13.0 ± 0.2 °C, a stable MAS frequency between 2000 and 2500 Hz, and using a <sup>2</sup>H-lock with high sensitivity detection. The latter is due to the use of a doubly tuned <sup>1</sup>H and <sup>2</sup>H µcoil, offering a high filling factor detection.

The µcoil of the HRµMAS probe<sup>11</sup> features a 10-turn solenoid. The unloaded quality factor at 600 MHz is 150, with a B<sub>1</sub>/P<sup>0.5</sup> efficiency of 1.14 mT W<sup>-1/2</sup> (where B<sub>1</sub> is the radio frequency field

at a given transmitter power  $P$ ). The solenoid provides excellent  $B_1$  field homogeneity over the sample region with  $I_{450^\circ}/I_{90^\circ} \approx 95\%$ .

Despite its small rotor size and light weight (11 mg including the sample), the probe is capable of having a long and stable spinning duration at frequencies lower than 3000 Hz. Fig. S2† shows a 10 hour sample spinning at a mean frequency of 2275 Hz with a stability of  $\pm 17$  Hz. Since the overall  $B_0$  inhomogeneity over the sample region is small (*i.e.*  $\sim 50$  Hz linewidth under non-spinning conditions), the small spinning fluctuation  $\pm 17$  Hz does not affect the NMR data.

### Spectral performance

Table 1 summarizes the detection sensitivity of the  $^1\text{H}$  spectra of the liver and brain extracts shown in Fig. 1. Despite the low concentration in 490 nl, high spectral sensitivities were obtained in just 27 minutes for the liver extract and in just 7 minutes for the brain extract with a resolution of about 5 ppb. The overall spectral-profiles correspond well to those of the HR-MAS spectra shown in Fig. S3.† The signal-to-noise ratio (SNR) of the rich-metabolite spectral region 2.5–4.5 ppm is  $71 \pm 12$  (mean  $\pm$  standard deviation) for the liver and  $84 \pm 19$  for the brain. These excellent spectral sensitivities and resolutions permit the identifications of about 15 metabolites in the liver and 20 in the brain. Impressively, with such low concentrations in nanoliter volumes, the spectra also reveal low-sensitive purine protons in adenosine triphosphate (or in inosine) at 6.14 and 8.22 ppm. A full list of the identified metabolites can be found in Table S1 in the ESI.† The limit of detection (LOD) and limit of quantification (LOQ) were estimated by taking the concentration of the extracts at  $\text{SNR} = 3$  and 10, respectively, and found to be below  $5 \mu\text{g } \mu\text{l}^{-1}$  and below  $20 \mu\text{g } \mu\text{l}^{-1}$ , respectively.

As shown clearly in Fig. 1, the well-separated individual metabolite signals such as lactate at 1.33 ppm, *N*-acetyl aspartate at 2 ppm and creatine at 3 ppm in the brain extract and glucose at 4.6 ppm in the liver extract could be used for determining the metabolite content by comparing the integral of the metabolite signals to a known quantity of an internal reference signal from either a chemical additive<sup>14</sup> or a digitally generated signal<sup>15</sup> (*i.e.* ERETIC2, Electronic Reference To access *In vivo* Concentrations).

To assess the spectral repeatability of each dataset (brain and liver), the RSD of the individual spectral bucket ( $\Delta = 0.01$  ppm) was calculated. Fig. 2A shows the RSD of the individual bucket intensity (of the four spectra) across the spectral

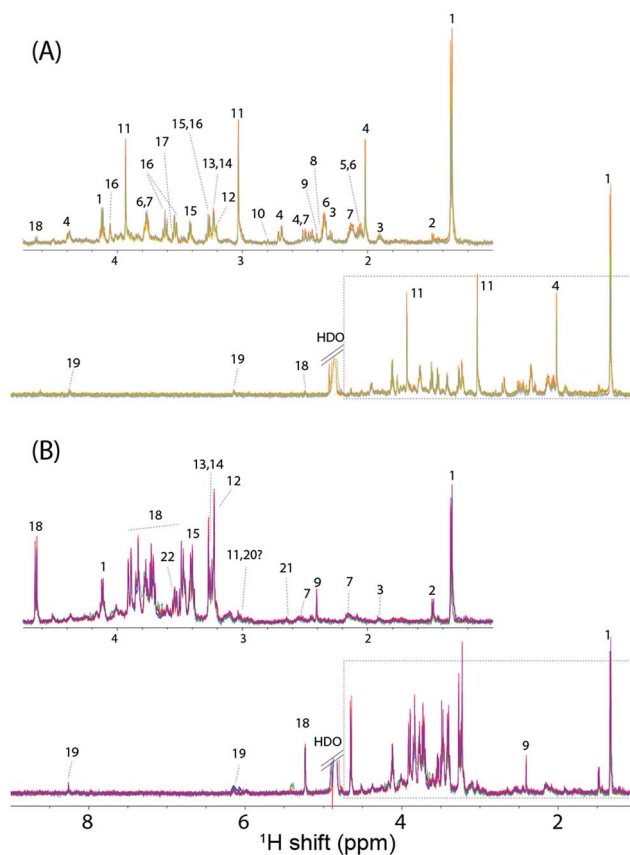


Fig. 1 Four overlaid  $^1\text{H}$  HR-MAS NMR spectra of the (A) brain and (B) liver extracts, with sample concentrations of  $<131$  and  $<41 \mu\text{g } \mu\text{l}^{-1}$ , respectively, in 490 nl. The tentative metabolite assignments: (1) lactate; (2) alanine; (3)  $\gamma$ -aminobutyric acid; (4) *N*-acetyl aspartate; (5) *N*-acetylaspartylglutamate; (6) glutamine; (7) glutamate; (8) pyruvate; (9) succinate; (10) aspartate; (11) creatine and phosphocreatine; (12) choline; (13) phosphorylcholine; (14) glycerophosphorylcholine; (15) taurine; (16) myo-inositol; (17) glycine; (18) glucose; (19) inosine and/or adenosine triphosphate; (20) lysine?; (21) citrate; (22) glycerol; HDO water.

region, highlighting the consistency of the low and high intensity peaks. The distribution of the RSD is shown as box-plots in Fig. 2B, offering a clear visual spectral variation within the group. It shows lines at the lower ( $-0.6745$  SD, where SD is the standard deviation), median and upper ( $+0.6745$  SD) quartile values. The black whiskers display the data within the range of  $\pm 2.698$  SD, while the red crosses are the outlier data points. A summary of the spectral RSD analyses can be found in Table 2.

Table 1 A summary of the spectral sensitivity for  $n = 4$

	Acqu. time (min)	Mean conc. ( $\mu\text{g } \mu\text{l}^{-1}$ )	Volume (nl)	SNR <sup>a</sup>	LOD <sup>b</sup> ( $\mu\text{g } \mu\text{l}^{-1}$ )	LOQ <sup>c</sup> ( $\mu\text{g } \mu\text{l}^{-1}$ )
Brain	7	131.5	490	$84 \pm 19$	$4.9 \pm 1.1$	$16.2 \pm 3.6$
Liver	27	41.5	490	$71 \pm 12$	$1.8 \pm 0.3$	$6.0 \pm 1.1$

<sup>a</sup> Mean signal-to-noise ratio  $\pm$  standard deviation over the spectral region of 2.5–4.5 ppm. <sup>b</sup> Limit of detection at 3 : 1 SNR. <sup>c</sup> Limit of quantification at 10 : 1 SNR.

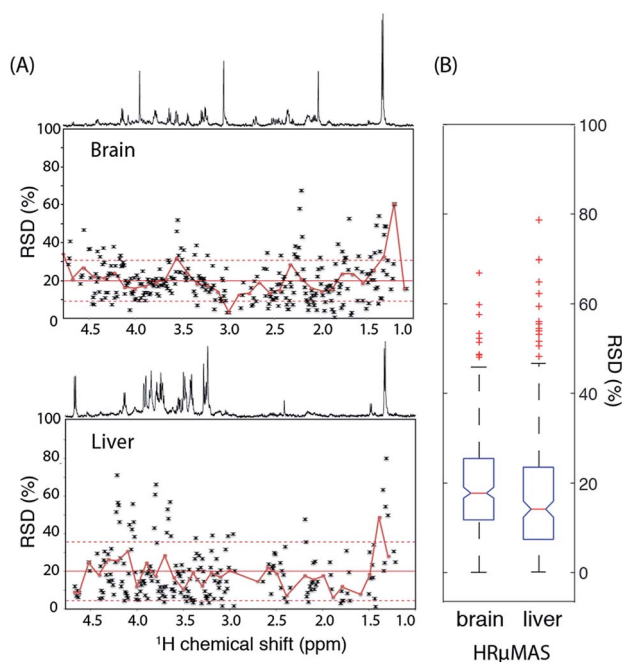


Fig. 2 Spectral RSD analysis. (A) The calculated RSD values of the individual bucket intensity ( $\Delta = 0.01$  ppm) of the four spectra across the spectral region 1.00–4.75 ppm. The red trendline (with a running mean of every 10 buckets) highlights the RSD variation. The red horizontal solid line indicates the mean RSD of the entire spectral region, with its standard deviations as dashed lines. (B) Boxplot of the RSD values summarizing the lower, median and upper quartiles, with the black whiskers displaying the range of data, and the red cross indicating the outlier data points. A summary of the RSD values can be found in Table 2.

Acceptable spectral variations are found within the four sampling spectra with a median RSD of 18.2% for the brain and 15.5% for the liver. This spectral variation is attributed to the fact that the entire sample volume is restricted in the detection coil region and that air bubbles are easily created during sample preparation leading to a slight  $B_0$  deviation over the sample region. One could re-shim to improve the  $B_0$  homogeneity for each data collection, but this can be tedious for a large-scale sampling. Another approach is to redesign the sample rotor in such a way that the sample volume is extended outside the detection coil region; in this way, any air bubbles created

Table 2 A summary of the spectral RSD analyses with  $n = 4$

RSDs in %	Brain	Liver
# of signal buckets <sup>a</sup>	283	209
Bucket spectra	1.00–4.75 ppm	1.00–4.75 ppm
RSD range	0.3–67.5	1.4–79.9
Mean RSD	20.1	19.7
Medium RSD	18.2	15.5
Standard deviation	11.2	14.8

<sup>a</sup> After the removal of the noise level. The procedure is described in the text.

outside the detection volume would not affect the spectral resolution; this would also offer a uniform sample detection volume and ease the quantitative analyses.

As anticipated, the spectral-profile shown in Fig. 1 is very different between the two extracts; large signals of lactate,  $\gamma$ -aminobutyric acid, creatine and phosphorylcholine (or glycerophosphocholine) are found in the brain, while the lactate and glucose signals dominate in the liver. Trace levels of alanine, glutamate and succinate are found in both. With these spectral differences, the multivariate data analyses (Fig. 3) are expected to show a clear metabolic differentiation between the two datasets. Indeed, the unsupervised PCA score plot not only reveals partitioning into two discrete clusters corresponding to the different extract groups, but also shows the data variations within the groups. The datasets were also subjected to a supervised statistical analysis using OPLS-DA. The corresponding S-line plot displays a metabolic variation between the two datasets (liver vs. brain). It reveals that the liver extract contains a significant amount of glucose and choline moieties as compared to the brain extract. Glucose concentration in the brain has been previously found to be between 0.8 and 1.6 mM,<sup>16</sup> whereas the liver, which takes up and stores glucose to minimize the fluctuation of glycaemia, is known to possess glucose contents between 8 and 11 mM, depending on the postprandial or fasted state.<sup>17</sup> These differences in the glucose content are evident in Fig. 1 and 3.

### Detection of $^1\text{H}$ - $^{13}\text{C}$ J-coupling

Before dissection, the rat was perfused for one hour with a solution of 750 mM glucose and 534 mM [ $3\text{-}^{13}\text{C}$ ]-labelled lactate. The liver is expected to intake the perfused metabolites, glucose and lactate, since this organ is involved in the Cori cycle, a metabolic loop that recycles the lactate anaerobically produced in the muscle. Hence, the  $^{13}\text{C}$ -labelled lactate makes it possible to trace the perfused lactate in the extracts by  $^{13}\text{C}$ -NMR. Fig. 4 shows the  $^1\text{H}$  doublet of the lactate- $\text{CH}_3$  signal at 1.33 ppm in the liver and brain extracts. The  $^{13}\text{C}$ - $^1\text{H}$  J splitting of 128 Hz is visible in both spectra. The peak integral of the splitting is ascribed to the sum of the perfused [ $3\text{-}^{13}\text{C}$ ] lactate

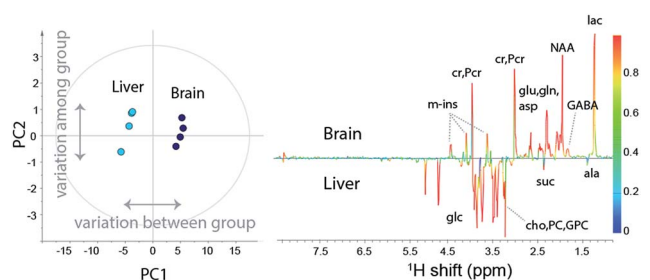


Fig. 3 Multivariate data analyses. (left) A PCA score plot of all datasets showing the quality of the subspectra with  $R2X(\text{cum}) = 0.955$ ;  $Q2(\text{cum}) = 0.902$ . (right) An OPLS-DA S-line plot with  $Q2 = 0.994$ ,  $R2Y(\text{cum}) = 0.999$  and  $R2X(\text{cum}) = 0.955$ . The positive peaks correspond to the metabolites in higher concentrations for the brain extract, while the negative peaks correspond to the higher content of metabolites for the liver extract.

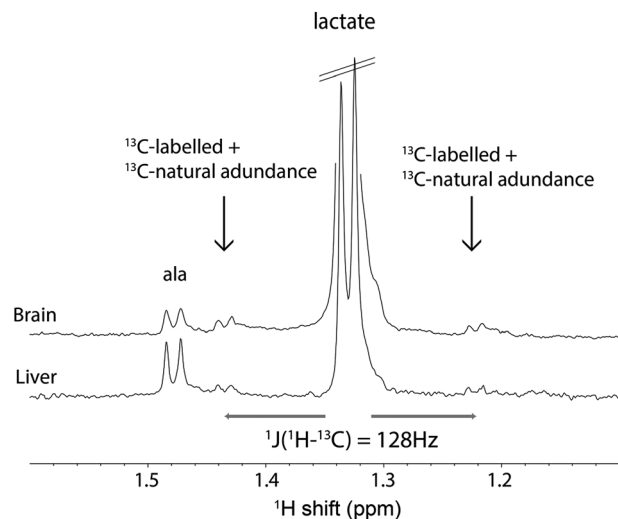


Fig. 4 An expanded spectral region 1.1–1.6 ppm showing the  $^1\text{H}$  doublet of lactate at 1.33 ppm and its  $^1\text{H}$ – $^{13}\text{C}$   $J$ -splitting. The spectra are the summation of all four corresponding individual spectra of the liver and brain shown in Fig. 1.

and the natural abundance  $^{13}\text{C}$  lactate; therefore, the content of the perfused lactate can be estimated by the integral ratio between the splitting and the total sum. The perfused [ $3\text{-}^{13}\text{C}$ ] lactate is found to be around 6.9% in the liver and 4.7% in the brain. The value found in the brain is higher than the  $^{13}\text{C}$  natural abundance 1.1%, suggesting that the perfused  $^{13}\text{C}$ -labeled lactate indeed passes through the blood–brain barrier and enters the brain, and plays a role in brain metabolism as a metabolic substrate.<sup>12,18</sup>

### Sample preparation

Sample preparation is an important aspect in metabolomic studies; the procedure must be clean and quick so as to keep the specimens in the utmost original state before data acquisitions. Unlike with large sample volumes, packing a tiny sample into a 1 mm diameter rotor can be a demanding task that requires working under a stereomicroscope with great care. Even though inexpensive Kel-F rotors are used as disposable rotors for a quick clean-up,<sup>11</sup> the current rotor design is not practical for a quick sample preparation procedure. Sealing the rotor is complicated because three specific plugs are necessary, two inserts and one cap, which are small and fragile. Moreover, the sealing procedure requires dedicated tools (Fig. S1†) to assist in the sealing and to ensure a good closure of the rotor without damaging the rotor. As a consequence, sealing the rotor is time-consuming and demands significant concentration. For instance, the sample preparation took about 20–30 minutes, of which over 90% was spent on sealing the rotor. Despite minimal sample degradations in the bio-extracts used in the study, we do acknowledge that such a lengthy sample preparation is not suitable for studying living specimens, in which the metabolic activities are expected to be fast. Nonetheless, the current performances of HR $\mu$ MAS are sufficient for performing studies on metabolically stable samples.

## Concluding remarks

The study presented here demonstrates that the stand-alone HR $\mu$ MAS probe can provide excellent detection sensitivity and spectral resolution, which are of prime importance for NMR metabolic profiling of nanoliter samples. The probe is robust and practical, and it can perform experiments under a controlled environment –  $B_0$  stabilization with a  $^2\text{H}$ -lock, probe temperature regulation and stable sample spinning – reproducing the standard HR-MAS experiments.

As demonstrated in the previous report,<sup>11</sup> 2D NMR experiments can be carried out readily for peak assignments. Heteronuclear NMR experiments can also be performed for targeted metabolite investigations. For example,  $^{13}\text{C}$ -edited/ $^1\text{H}$ -observed NMR-pulse experiments could be used for tracing and quantifying the infused labelled  $^{13}\text{C}$ -substrates in living metabolism.<sup>12</sup>

This evaluation has also helped to reveal practical difficulties with the sample preparation for HR $\mu$ MAS experiments. In this regard, we are currently working on new rotor designs that would simplify and shorten the sample preparation procedure. We anticipate that HR $\mu$ MAS has the potential to become a truly convenient NMR-based spectroscopic approach to investigate metabolic problems that could not be addressed before and it could open a new framework in NMR-based metabolomics.

## Acknowledgements

We would like to thank the French National Research Agency for financial support under ANR-12-JSV5-0005 (ANR33HRMACSZ) and JEOL RESONANCE Inc. AKBS is supported by ANR-10-LABX-57 (TRAIL). We are also grateful to Dr Manoj Kumar Pandey (RIKEN) for his assistance in sample preparation and sample spinning.

## Notes and references

- O. Beckonert, M. Coen, H. C. Keun, Y. Wang, T. M. D. Ebbels, E. Holmes, J. C. Lindon and J. K. Nicholson, *Nat. Protoc.*, 2010, **5**, 1019–1032.
- H. Janssen, A. Brinkmann, E. R. H. van Eck, P. J. M. van Bentum and A. P. M. Kentgens, *J. Am. Chem. Soc.*, 2006, **128**, 8722–8723.
- D. Sakellariou, G. Le Goff and J. F. Jacquinot, *Nature*, 2007, **447**, 694–697.
- A. Wong, B. Jiménez, X. Li, E. Holmes, J. K. Nicholson, J. C. Lindon and D. Sakellariou, *Anal. Chem.*, 2012, **84**, 3843–3848.
- Y. Nishiyama, Y. Endo, T. Nemoto, H. Utsumi, K. Yamauchi, K. Hioka and T. Asakura, *J. Magn. Reson.*, 2011, **208**, 44–48.
- Bruker, *56th Experimental Nuclear Magnetic Resonance Conference*, 2015, April 10–15.
- J. Feng, J. Z. Hu, S. D. Burton and D. W. Hoyt, *Chin. J. Magn. Reson.*, 2013, **30**, 1–11.
- A. Wong, X. Li and D. Sakellariou, *Anal. Chem.*, 2013, **85**, 2021–2026.
- A. Wong, C. Boutin and P. M. Aguiar, *Front. Chem.*, 2014, **2**, 38.

- 10 A. Wong, X. Li, L. Molin, F. Solari, B. Elena-Herrmann and D. Sakellariou, *Anal. Chem.*, 2014, **86**, 6064–6070.
- 11 Y. Nishiyama, Y. Endo, T. Nemoto, A. K. Bouzier-Sore and A. Wong, *Analyst*, 2015, **140**, 8097–8100.
- 12 A. K. Bouzier, E. Thiaudiere, M. Biran, R. Rouland, P. Canioni and M. Merle, *J. Neurochem.*, 2000, **75**, 480–486.
- 13 H. M. Parsons, D. R. Ekman, T. W. Collette and M. R. Viant, *Analyst*, 2009, **134**, 478–485.
- 14 M. G. Swanson, A. S. Zektzer, Z. L. Tabatabai, J. Simko, S. Jarso, K. R. Keshari, L. Schmitt, P. R. Carroll, K. Shinohara, D. B. Vigneron and J. Kurhanewicz, *Magn. Reson. Med.*, 2006, **55**, 1257–1264.
- 15 O. Frank, J. K. Kreissl, A. Daschner and T. Hofmann, *J. Agric. Food Chem.*, 2014, **62**, 2506–2515.
- 16 W. M. Abi-Saab, D. G. Maggs, T. Jones, R. Jacob, V. Srihari, J. Thompson, D. Kerr, P. Leone, J. H. Krystal, D. D. Spencer, M. J. During and R. S. Sherwin, *J. Cereb. Blood Flow Metab.*, 2002, **22**, 271–279.
- 17 P. A. Wals and J. Katz, *Metabolism*, 1993, **42**, 1492–1496.
- 18 D. Sampol, E. Ostrofet, M. L. Jobin, G. Raffard, S. Sanchez, V. Bouchaud, J. M. Franconi, G. Bonvento and A. K. Bouzier-Sore, *Front. Neuroenerg.*, 2013, **5**, 5.